Article

Textile Antenna with Dual Bands and SAR Measurements for Wearable Communication

Mahmoud A. Abdelghany [1,2,*], Mohamed I. Ahmed [3,4], Ahmed A. Ibrahim [2], Arpan Desai [5] and Mai. F. Ahmed [6]

1   Electrical Engineering Department, College of Engineering, Prince Sattam Bin Abdulaziz University, Wadi Addwasir 11991, Saudi Arabia
2   Electronics and Communications Engineering Department, Minia University, El-Minia 61519, Egypt; ahmedabdel_monem@mu.edu.eg
3   Electronics Research Institute, Microstrip Department Joseph Tito Str., Huckstep, El Nozha, Cairo 11843, Egypt; miahmed@eri.sci.eg or Mohamed.Ahmed@eui.edu.eg
4   Electronics and Communication Program, Faculty of Engineering, Egypt University of Informatics, Knowledge City, New Administrative Capital, Cairo 11865, Egypt
5   Department of Information and Communication Technology, Pandit Deendayal Energy University, Gandhinagar 382007, India; arpan.desai@sot.pdpu.ac.in
6   Department of Electronics and Comm. Engineering, Faculty of Engineering, Zagazig University, Zagazig 44519, Egypt; mfabdelhalim@eng.zu.edu.eg
*   Correspondence: ma.khalil@psau.edu.sa

Abstract: A novel dual-wideband textile antenna designed for wearable applications is introduced in this study. Embedding antennas into wearable devices requires a detailed analysis of the specific absorption rate (SAR) to ensure safety. To achieve this, SAR values were meticulously simulated and evaluated within a human voxel model, considering various body regions such as the left/right head and the abdominal region. The proposed antenna is a monopole design utilizing denim textile as the substrate material. The characterization of the denim textile substrate is carried out using two different methods. The first analysis included a DAC (Dielectric Assessment Kit), while a ring resonator technique was employed for the second examination. Operating within the frequency bands of (58.06%) 2.2–4 GHz and (61.43) 5.3–10 GHz, the antenna demonstrated flexibility in its dual-wideband capabilities. Extensive simulations and tests were conducted to assess the performance of the antenna in both flat and bent configurations. The SAR results obtained from these tests indicate that the antenna complies with safety standard limits when integrated with the human voxel model. This validation underscores the potential of the proposed antenna for seamless integration into wearable applications, offering a promising solution for future developments in this domain.

Keywords: dual wideband; monopole antenna; SAR testing; textile substrate; wearable application

1. Introduction

Wearable antennas represent a critical frontier in the intersection of technology and healthcare, offering a plethora of benefits in real-time monitoring and communication within medical contexts. These antennas, seamlessly integrated into wearable devices, play a pivotal role in continuously and discreetly tracking vital signs and other health metrics. The significance of this innovation reverberates across academic and industrial domains, particularly in the realm of wireless body area network (WBAN) systems, with applications spanning healthcare, sports, security, and military sectors [1].

The utilization of textile substrates, such as felt and denim, in the fabrication of wearable antennas is motivated by their low dielectric constant (εr), which enhances the impedance bandwidth of the antenna radiator [2]. Among the myriad textile options, wearable antennas crafted from felt and denim stand out for WBAN applications, offering a suite of advantages including lightweight composition, flexibility, cost-effectiveness

for printing, and hardware simplicity [3,4]. Recent advancements have witnessed the emergence of various wearable and flexible antenna designs, encompassing wideband monopole antennas [5–7], fractal slotted antennas with loaded metamaterials [8], ultra-wideband (UWB) antennas [9,10], and metasurface-based wearable planar inverted-F antennas (PIFA) [11].

The selection between dual wideband and ultra-wideband antennas hinges upon several factors, including the specific frequency requisites of the application, the necessity of versatility, interference mitigation, and desired data rates. Each antenna topology presents unique advantages and trade-offs, necessitating a judicious consideration of the application requirements to determine the most suitable option. In essence, wearable antennas represent a transformative technology poised to revolutionize healthcare and beyond, offering unprecedented capabilities for seamless and unobtrusive monitoring in diverse settings. With ongoing research and innovation, the landscape of wearable antennas continues to evolve, promising enhanced performance and expanded applications in the foreseeable future. The realm of modern healthcare technology is witnessing a surge in proposals for ultra-wideband (UWB) wearable radiators, with several notable contributions documented in recent literature [12–15]. Among these advancements, dual wideband antennas have emerged as pivotal components in biomedical wearable applications, offering a unique capability to operate across multiple frequency bands. This versatility opens avenues for a diverse range of applications within the biomedical field, where continuous monitoring and communication are paramount.
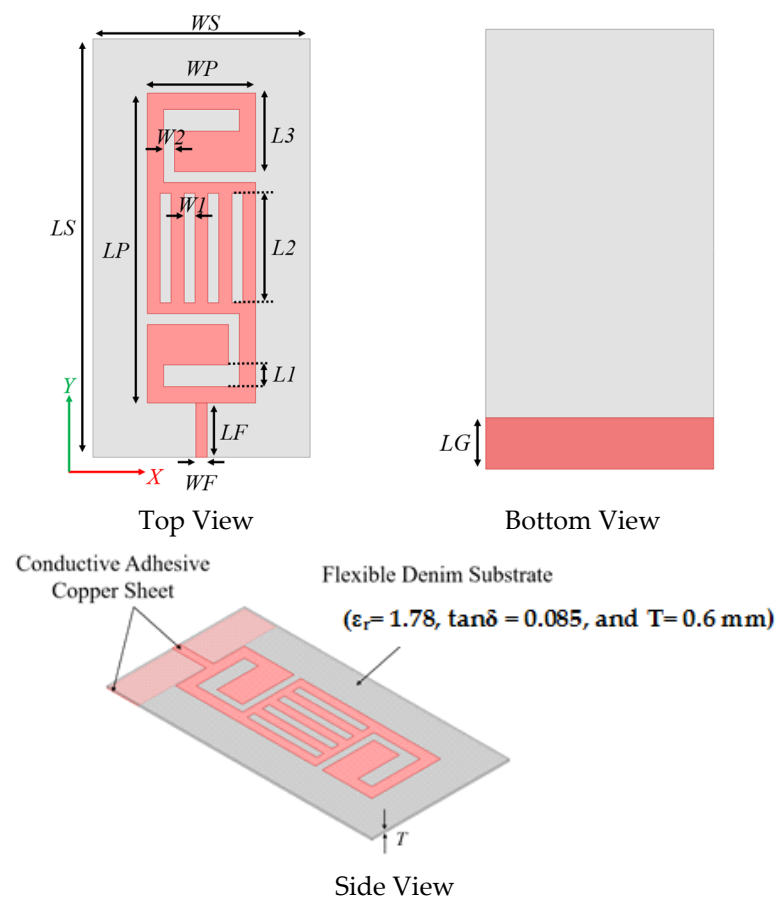
The integration of dual wideband antennas brings forth a multitude of benefits, including enhanced frequency coverage, support for multi-modal sensing, improved reliability, and compatibility with emerging technologies. These antennas play a crucial role in remote patient monitoring and the evolution of personalized healthcare, heralding the development of innovative and effective medical devices [16–23]. In specific studies such as [16,17], flexible antennas designed for body-centric and WLAN applications utilize substrates like nitrile butadiene rubber and felt, with thicknesses ranging from 4.6 mm to 5 mm. However, the use of relatively thick substrates may pose challenges in achieving the required flexibility for seamless integration into wearable devices. Addressing this demand for flexibility, Refs. [18,19] propose semi-flexible antennas based on Rogers substrates tailored for WBAN applications, catering to the growing need for substrates with higher tensile strength. In the pursuit of flexible yet robust substrates, Ref. [20] explores rubber as a substrate for antennas, although a comprehensive bending analysis is notably absent. Conversely, Refs. [21,22] introduce antennas employing cellulose laurate and polyimide substrates, conducting thorough bending analyses and achieving commendable gains. However, these designs exhibit narrower bandwidths, with [21] highlighting the necessity for higher bandwidth designs to cater to a broader range of applications. It is worth noting that while simulated specific absorption rate (SAR) studies have been conducted for the discussed dual-band antennas, none have undergone actual SAR measurements, indicating a potential area for future research and validation. As the field of wearable antennas continues to evolve, addressing these challenges will be crucial in unlocking their full potential in revolutionizing healthcare technology.

In this paper, we address the limitations observed in existing wearable antennas by proposing a dual-wideband monopole antenna with flexible and wearable features for WBAN applications. Fabricated on a flexible and thin denim textile material, the radiator covers an extensive bandwidth from 2.2 to 4 GHz and 5 to 10 GHz, respectively. Denim, chosen as the substrate, surpasses other materials like rubber, cellulose laurate, and polyimide in wearable applications due to its exceptional combination of lightweight construction, flexibility, and cost-effectiveness for printing. Notably, the antenna exhibits stability under various bending conditions, ensuring its adaptability to diverse body shapes. Furthermore, specific absorption rate (SAR) levels were simulated and tested on a human voxel model for both the left/right head and the stomach, respectively. The measured SAR values align with safety standards, endorsing the proposed denim-based antenna

as a superior and viable solution for wearable applications in healthcare. The paper is arranged as follows: the introduction is the first section of the paper; the second part contains the flexible antenna configuration, antenna evolution, and parametric studies of its design parameters. The results and discussions of the antenna under both the bending and normal conditions are investigated in Section 3. Section 4 presents the SAR calculations and measurements using both the EM simulation and the cSAR3D system. Finally, the conclusion of the paper is presented in Section 5.

2. Antenna Geometry

The flexible wearable radiator geometry is illustrated in Figure 1. This antenna is characterized as a flexible monopole featuring a partial ground plane. Both the monopole radiator and the partial ground plane are etched onto distinct sides of a denim textile substrate. Two methods are employed to assess the dielectric properties of the denim fabric. The first method utilizes DAC equipment (Dielectric Assessment Kit), while a ring resonator technique is involved for the second analysis [23,24]. These techniques enable precise measurement and evaluation of the denim fabric's dielectric characteristics, which is crucial for optimizing the performance of the wearable antenna.

Figure 1. Antenna Geometry.

Figure 2 depicts the evolutionary progression of the wearable antenna design, starting from the initial configuration (ant #1) to the anticipated design (ant #4). Ant #1 is characterized by a rectangular radiator and a partial ground plane situated on both sides of the substrate. It operates within the frequency range of 3.5–8 GHz, with S11 $\leq$ −10 dB, as illustrated the red dotted line. To extend the lower- and upper-frequency bands, antenna #2 incorporates two C-shaped etchings on the rectangular radiator, operating from 2.2 to 10 GHz. Additionally, the green dashed line indicates a notch band with S11 $\leq$ −4 dB from 4 to 5.5 GHz. In the third design iteration (antenna #3), the rectangular radiator is

enhanced with two rectangular slots. The antenna operates from 2.2 to 9 GHz, featuring a notch band with S11 ≤ −7 dB from 4 to 5 GHz, denoted by the blue dashed–dotted line. The suggested antenna (antenna #4) further improves performance by incorporating four rectangular slots alongside two inverted C-shaped etchings, as illustrated in Figure 3. Operating from 2.2 to 10 GHz, this design introduces a notch band with S11 ≤ −7 dB from 4–5.3 GHz, represented by the black solid line. Table 1 presents the optimum dimensions for reference and analysis.

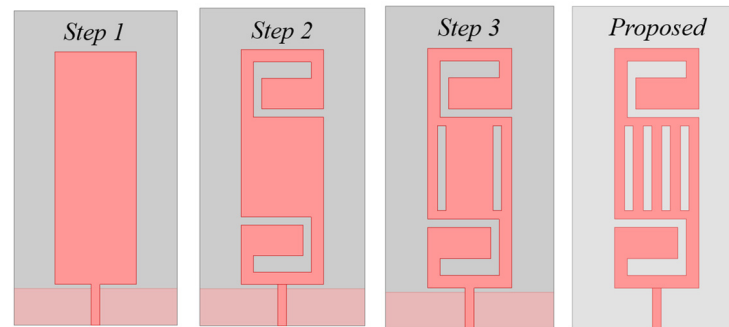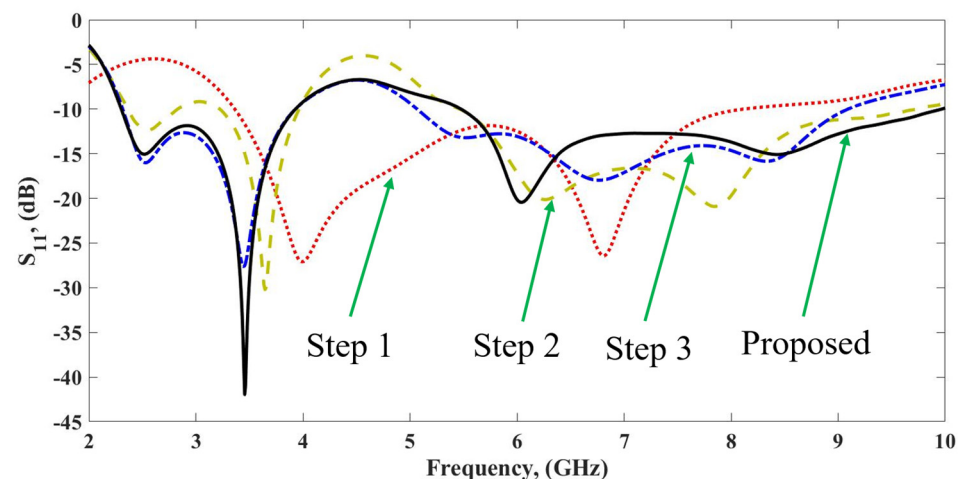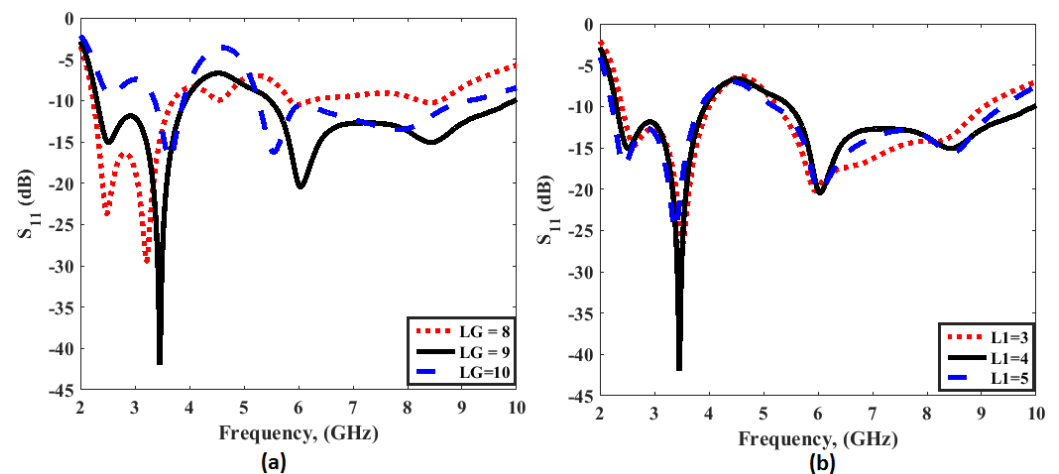**Figure 2.** Antenna evolution.

Figure 3. Reflection coefficient analysis of antenna evolution.

Table 1. The wearable antenna dimensions.

LS	WS	WP	LP	WF	LF
77	40	20	57	2.12	10
LG	L1	L2	L3	W1	W2
9	4	20.2	14.4	2	2

Parametric studies were utilized to demonstrate the effect of antenna dimensions on the reflection coefficient. Figure 4a illustrates the impact of ground length (LG) on the reflection coefficient. The length of the partial ground (LG) affects antenna matching, necessitating careful selection to achieve desired outcomes. When the ground length LG = 8 mm, the antenna exhibits good matching at the lower frequency band, with $S_{11} \leq$ −10 dB extending from 2 GHz to 3.5 GHz, and reaching −10 dB from 3.6 GHz to 9 GHz. Antenna matching is compromised when LG = 10 mm, as depicted in Figure 4a. The optimal case occurs when LG = 9 mm, with the antenna displaying $S_{11} \leq$ −10 dB from 2.2 to 4 GHz and 5.3 to 10 GHz.
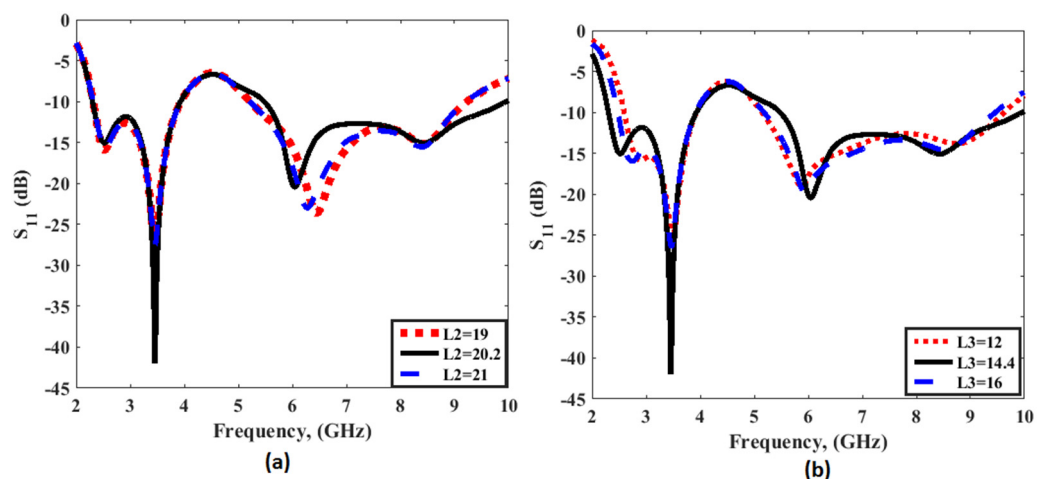
Figure 4. The effect of the antenna dimensions on the reflection coefficient (**a**) LG (**b**) L1.

Figure 4b demonstrates the effect of L1 on the reflection coefficient. With L1 = 3 mm, the antenna shows $S_{11} \leq -10$ dB from 2.2 to 4 GHz and 5.3 to 8.5 GHz. Increasing L1 to 4 mm extends the range of good matching from 2.2 to 4 GHz and 5.3 to 10 GHz. Finally, with L1 = 5 mm, the antenna exhibits $S_{11} \leq -10$ dB from 2.2 to 4 GHz and 5.3 to 9 GHz. Therefore, L1 = 4 mm was selected as the optimal length.

The effect of L2 on the reflection coefficient is illustrated in Figure 5a. When the length of L2 = 19 mm (the red dotted line), the antenna operates from 2.2 to 4 GHz and 5.2 to 9 GHz with $S_{11} \leq -10$ dB. With a length of L2 = 20.2 mm (the black solid line), the antenna operates from 2.2 to 4 GHz and 5.3 to 10 GHz with $S_{11} \leq -10$ dB. Similarly, when L2 = 21 mm (the blue dashed line), the antenna operates from 2.2 to 4 GHz and 5.2 to 9 GHz with $S_{11} \leq -10$ dB. Therefore, L2 = 20.2 mm was selected to achieve the desired results.
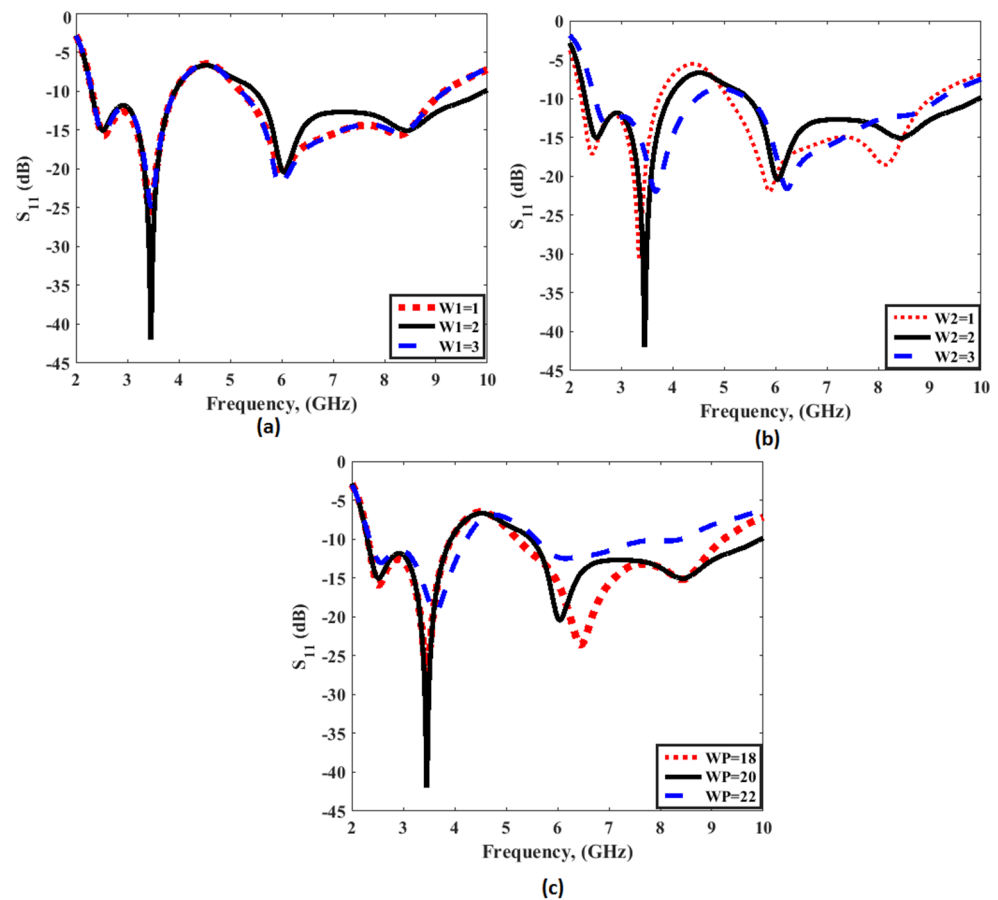

Figure 5. The effect of the antenna dimensions on the reflection coefficient (**a**) L2 (**b**) L3.

Additionally, the effect of L3 on the reflection coefficient is depicted in Figure 5b. With a length of L3 = 12 mm (the red dotted line), the antenna operates from 2.5 to 4 GHz and 5.2 to 9.6 GHz with $S_{11} \leq -10$ dB. Increasing L3 to 14.4 mm (the black solid line), the antenna operates from 2.2 to 4 GHz and 5.3 to 10 GHz with $S_{11} \leq -10$ dB. Subsequently, when L3 = 16 mm (the blue dashed line), the antenna operates from 2.4 to 4 GHz and 5.2 to 9.5 GHz with $S_{11} \leq -10$ dB. Hence, L3 = 14.4 mm was chosen to achieve the specified results.

The effect of W1 on the reflection coefficient is illustrated in Figure 6a. When the length of W1 = 1 mm (the red dotted line), the antenna operates from 2.2 to 4 GHz and 5.2 to 9 GHz with $S_{11} \leq -10$ dB. With W1 = 2 mm (the black solid line), the antenna operates

from 2.2 to 4 GHz and 5.3 to 10 GHz with $S_{11} \leq -10$ dB. Similarly, with W1 = 3 mm (the blue dashed line), the antenna operates from 2.2 to 4 GHz and 5.2 to 9 GHz with $S_{11} \leq -10$ dB. Therefore, W1 = 2 mm was selected to achieve the desired outcomes.
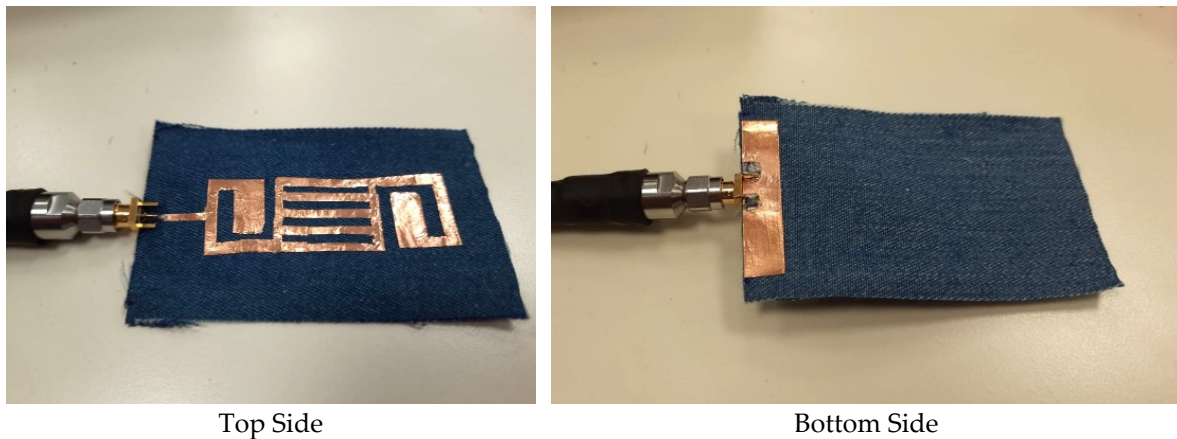

Figure 6. The effect of the antenna dimensions on the reflection coefficient (**a**) W1 (**b**) W2 (**c**) WP.

Additionally, the effect of W2 on the reflection coefficient is illustrated in Figure 6b. When the length of W2 = 1 mm (the red dotted line), the antenna operates from 2.1 to 3.9 GHz and 5.1 to 8.9 GHz with S11 ≤ -10 dB. With W2 = 2 mm (the black solid line), the antenna operates from 2.2 to 4 GHz and 5.3 to 10 GHz with $S_{11} \leq -10$ dB. Furthermore, with W2 = 3 mm (the blue dashed line), the antenna operates from 2.4 to 5 GHz and 5.3 to 8.9 GHz with $S_{11} \leq -10$ dB. Hence, W2 = 2 mm was chosen to achieve the required results. Finally, the effect of WP on the reflection coefficient is illustrated in Figure 6c. When the length of WP = 18 mm (the red dotted line), the antenna operates from 2.2 to 4 GHz and 5.3 to 9 GHz with $S_{11} \leq -10$ dB. With WP = 20 mm (the black solid line), the antenna operates from 2.2 to 4 GHz and 5.3 to 10 GHz with $S_{11} \leq -10$ dB. Additionally, with WP = 22 mm (the blue dashed line), the antenna operates from 2.4 to 4.2 GHz and 5.3 to 8.6 GHz with $S_{11} \leq -10$ dB. Thus, WP = 20 mm was selected to achieve the desired results.
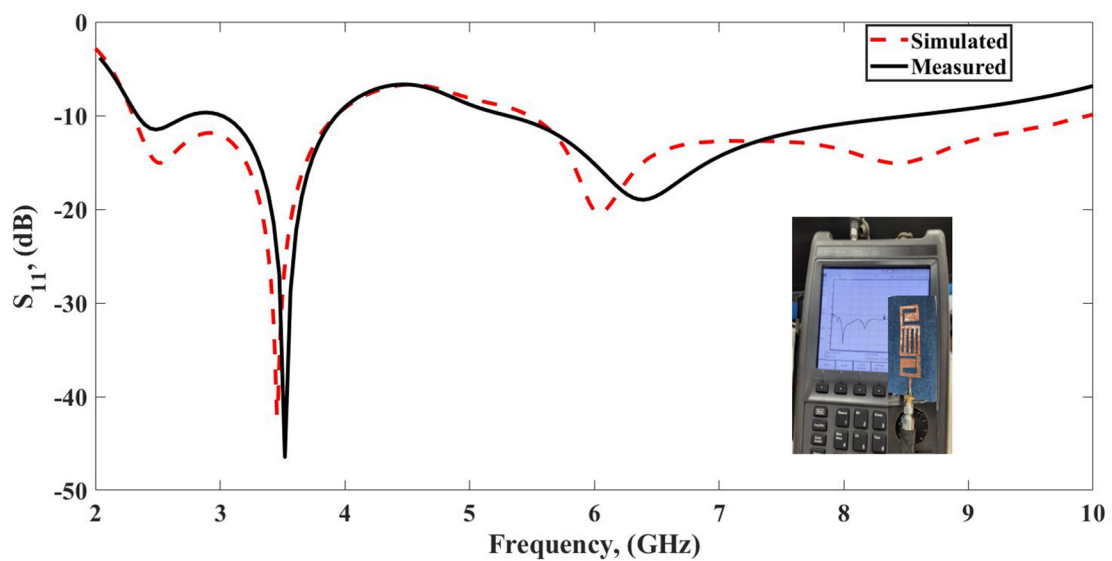
3. Results and Discussion

The testing of the flexible denim-based fabricated antenna, as depicted in Figure 7 where the top and bottom views are illustrated, was carried out. The S_{11} results were extracted to compare with the simulated outcomes for normal and bending conditions.

Top Side   Bottom Side

Figure 7. Fabricated prototype.

3.1. Under Normal Conditions

As depicted in Figure 8, the wearable antenna functions within the frequency range of 2.2–4 GHz and 5.3–10 GHz, rendering simulation data. Conversely, the experimental results indicate that the radiator resonates from 2.2 to 4 GHz and 5.3 to 9.5 GHz, achieving S_{11} values of ≤ -10 dB. Notably, both sets of outcomes exhibit a consistent trend, reinforcing the validity and effectiveness of the antenna design.

Figure 8. S_{11} of the wearable antenna.

To understand the radiator's performance across various frequency bands, an examination of the current distribution is conducted and illustrated in Figure 9. It is noticed that at 2.45 GHz, the current concentration is mainly around the C-shaped slots. In contrast, at 3.5 GHz and 5.8 GHz, the currents are concentrated around the rectangular slots.
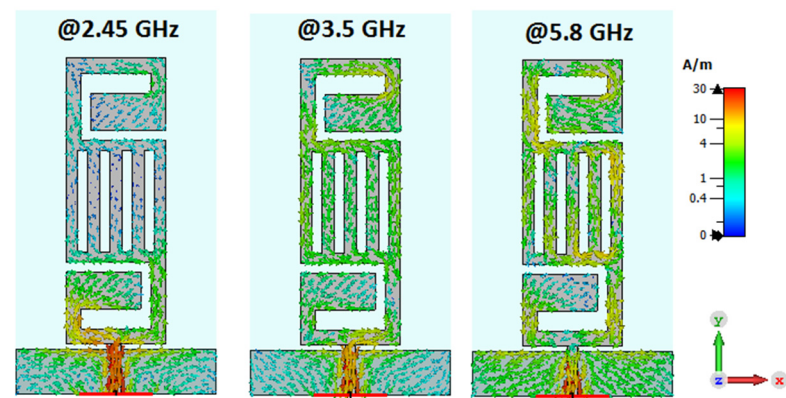
Figure 9. Current distribution.

The suggested antenna pattern measurement setup is demonstrated in Figure 10a. The antenna inside the chamber, as revealed in Figure 10b, was tested to measure its 2D patterns and gain. The proposed antenna under test (PAUT) was positioned in the line of sight to the horn antenna, as depicted in Figure 10. Surrounding absorbers within the chamber served to absorb any reflected electromagnetic (EM) waves. The PAUT underwent rotation in both the Azimuth and Elevation planes. A vector network analyzer (VNA) device was utilized to feed the horn antenna for radiation, after which the radiated EM waves were received by the PAUT. Finally, far-field radiation patterns were plotted using the installed computer software, and data on the EM radiation patterns were extracted and plotted, as illustrated in Figure 11. The normalized radiation patterns in both planes at three different bands are illustrated in Figure 11. The radiator had an omnidirectional pattern in both planes with reasonable agreements between the two outcomes.
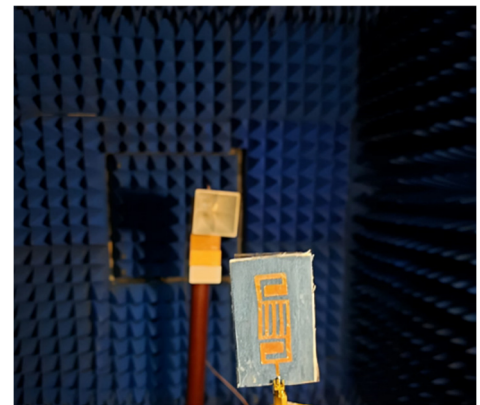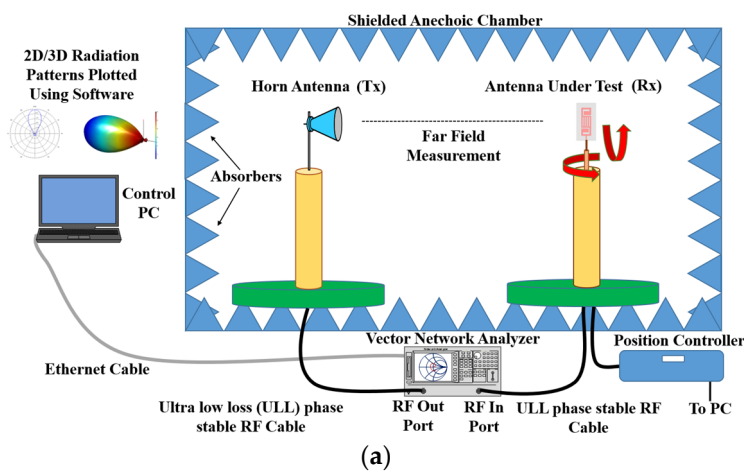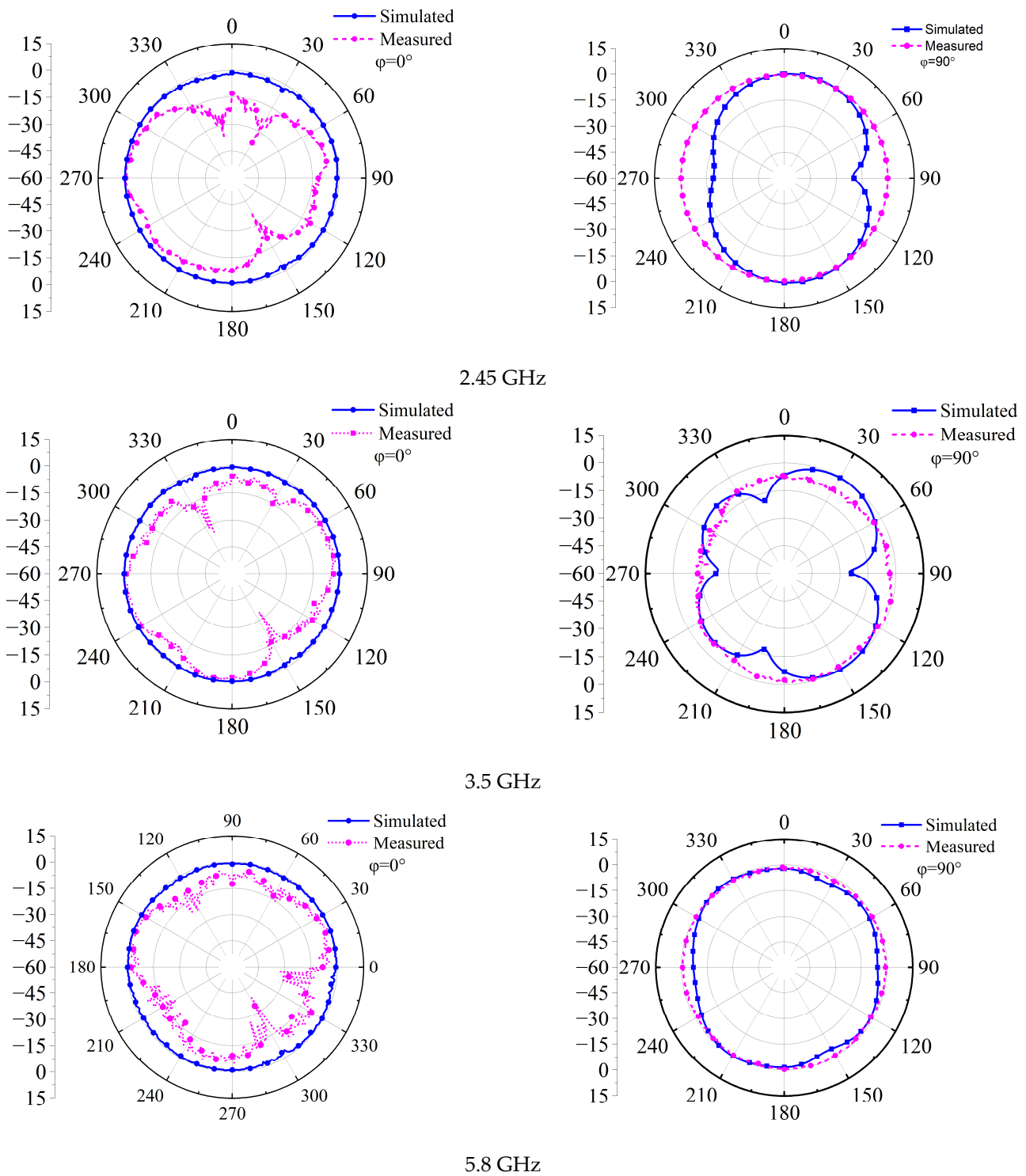

Figure 10. Radiation pattern measurement. (**a**) Test setup. (**b**) Inside the chamber.

2.45 GHz

3.5 GHz

5.8 GHz

Figure 11. Normalized radiation pattern.

As well, the simulated co-pol and cross-pol patterns are illustrated in Figure 12, where it can be observed that satisfactory results were achieved at the bands of interest.

Furthermore, the antenna gain is displayed in Figure 13. From this result, the antenna has simulated values between 2 and 4.5 dBi and measured results of 2–4.1 dBi, respectively, with a good trend between the two results.
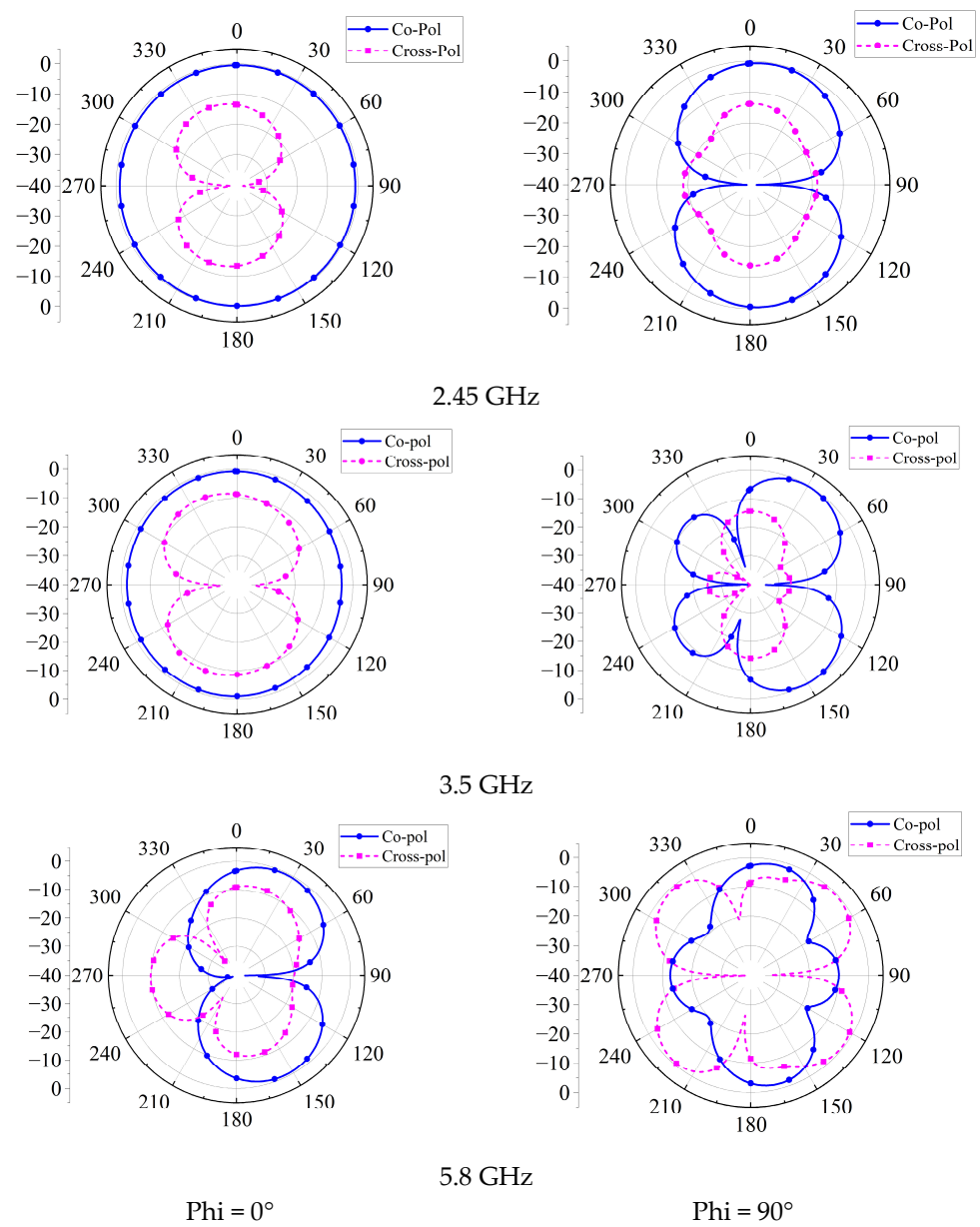
2.45 GHz

3.5 GHz

5.8 GHz

Phi = 0°   Phi = 90°

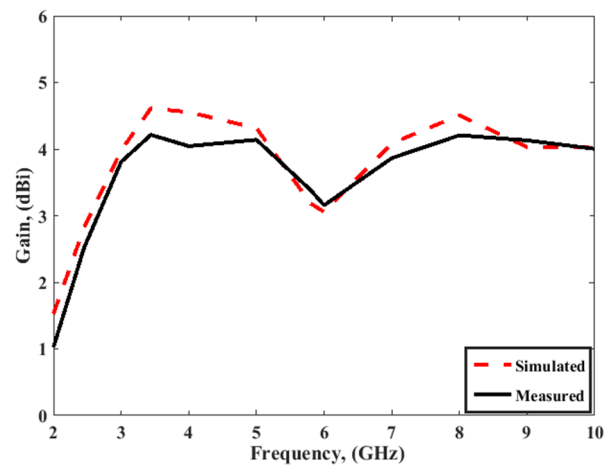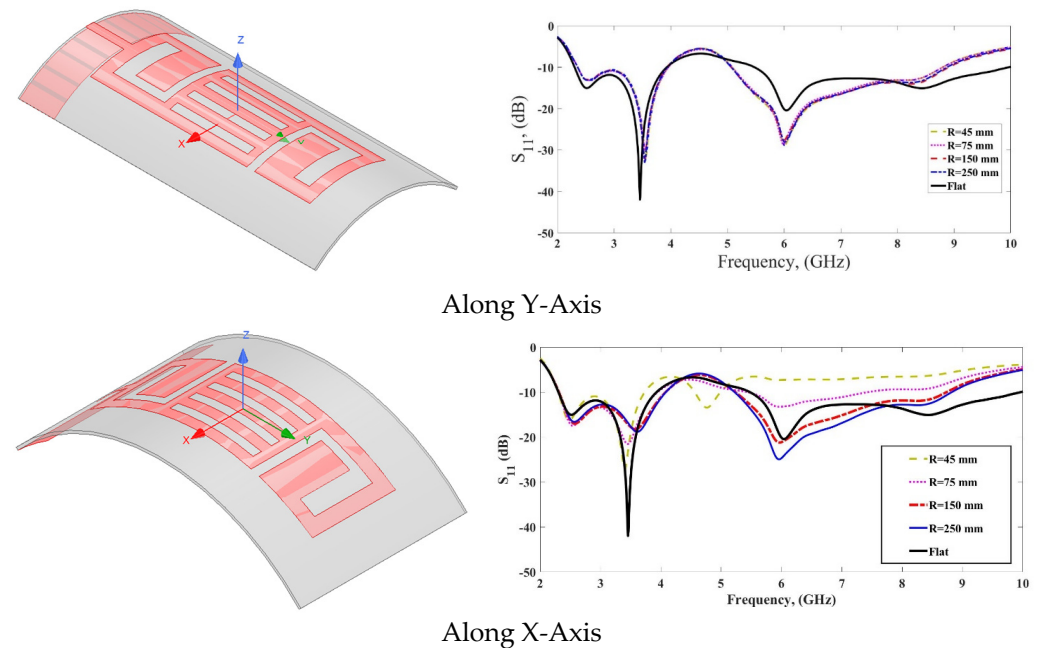**Figure 12.** Simulated co/cross pol results.

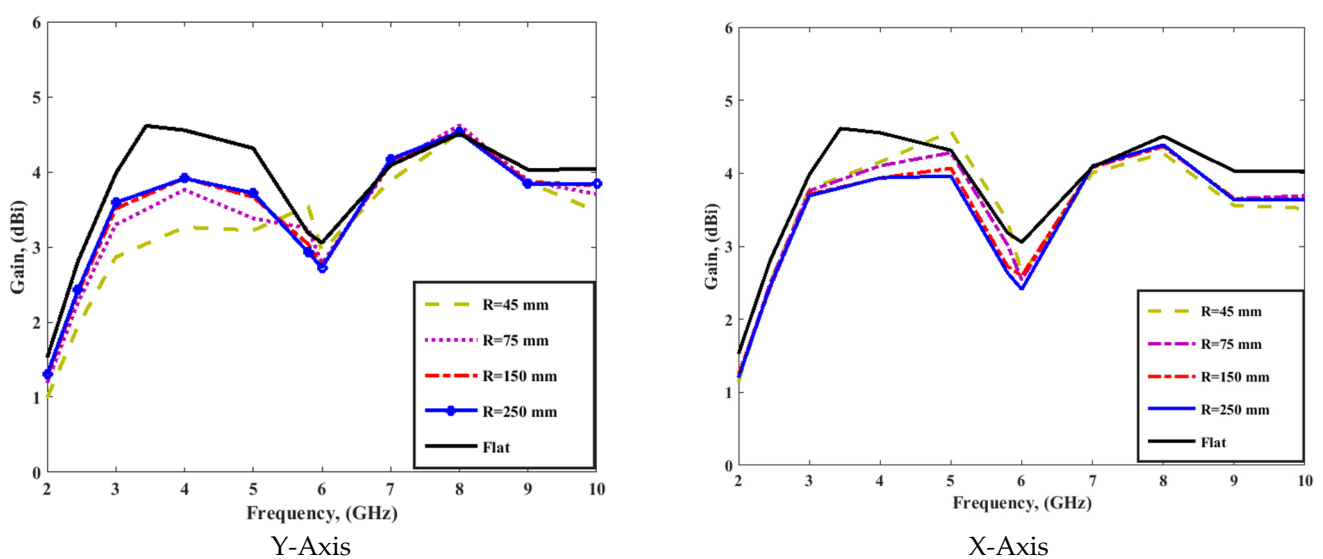**Figure 13.** The antenna gains in normal conditions (simulated and tested).

3.2. Bending Condition

To validate the stability, this design underwent bending with various radii around the *x*-axis and *y*-axis, as shown in Figure 14. The wearable radiator was slightly affected when the radius was larger than R = 45 mm. Since the proposed wearable antennas are intended for integration into the human body, the optimal choices for the head and stomach regions are radii of 150 mm and 250 mm. These selections are suitable for areas that do not require smaller radii.

Along Y-Axis

Along X-Axis

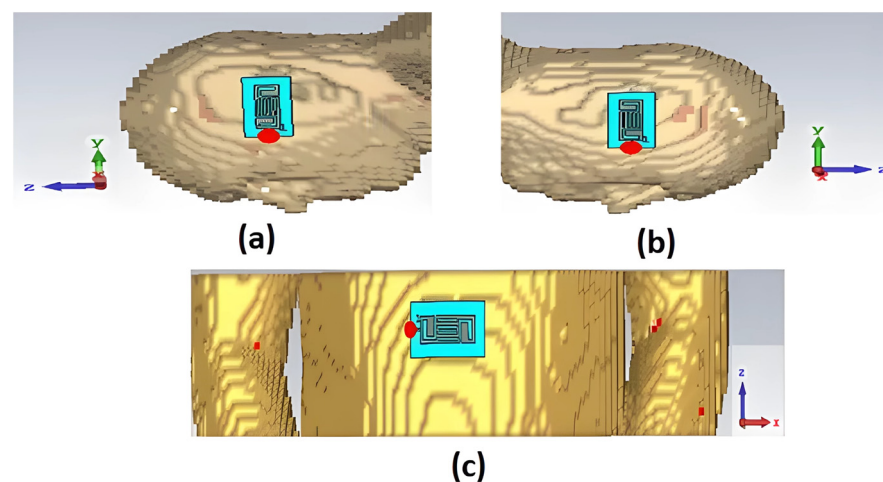**Figure 14.** S_{11} results of the wearable antenna under bending.

The gains under bending conditions exhibit minimal impact, as illustrated in Figure 15, contributing to the superior flexibility performance of the denim substrate. The gain values closely resemble those achieved in the normal case.

Y-Axis

X-Axis

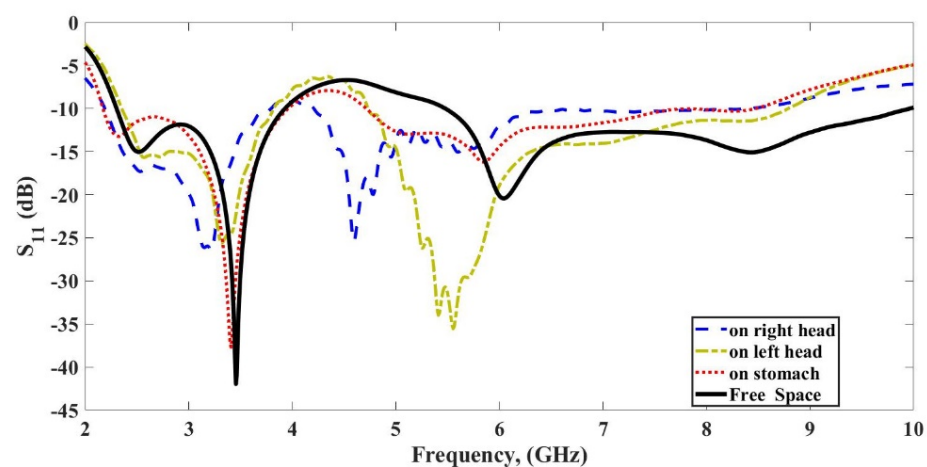**Figure 15.** The antenna gains under bending conditions.

4. Sar Calculation and Measurements

The SAR serves as the standard for evaluating the quantity of EM waves absorbed by tissues. The SAR is the standard level used to evaluate the electromagnetic waves soaked up by human tissues. Typical limits were established to show the safety levels of the SAR. The USA and EUROPE standards were used to judge the amount of the SAR levels. For the optimal design of wearable antennas, the SAR must remain below the established standards, such as the USA standard set by FCC at 1.6 W/kg and the EUROPE standard established by ICNIPR at 2 W/kg [22]. The voxelized human model was employed to replicate the human body in simulations. The antenna was affixed in three distinct positions (stomach, left, and right head), as depicted in Figure 16. The suggested antenna was positioned 5 mm away from the human voxel model.

Figure 16. Integration scenario on the human voxel model (**a**) left head, (**b**) right head, and (**c**) stomach.

The illustration in Figure 17 depicts the simulated S_{11} of the integrated radiator on the human voxel model. The antenna exhibits resonance within the frequency range of 2.2 GHz to 4 GHz and 4.5 GHz to 9 GHz when affixed to the human body model in three distinct positions (stomach, left, and right head). The free-space antenna results are displayed for comparison. Additionally, both results show a similar pattern with a minor shift, ascribed to the integration of the antenna with the human body, influencing the matching of radiator impedances.

Figure 17. The simulated S_{11} of the integrated radiator on the human voxel model.

The simulated antenna efficiency in different cases is shown in Figure 18. The radiation efficiency changed from around 65% to 95%, and the total efficiency changed from around

50% to 93% for all cases. Also, it is seen that the efficiency of the antenna is affected when the antenna is added close to the human body.
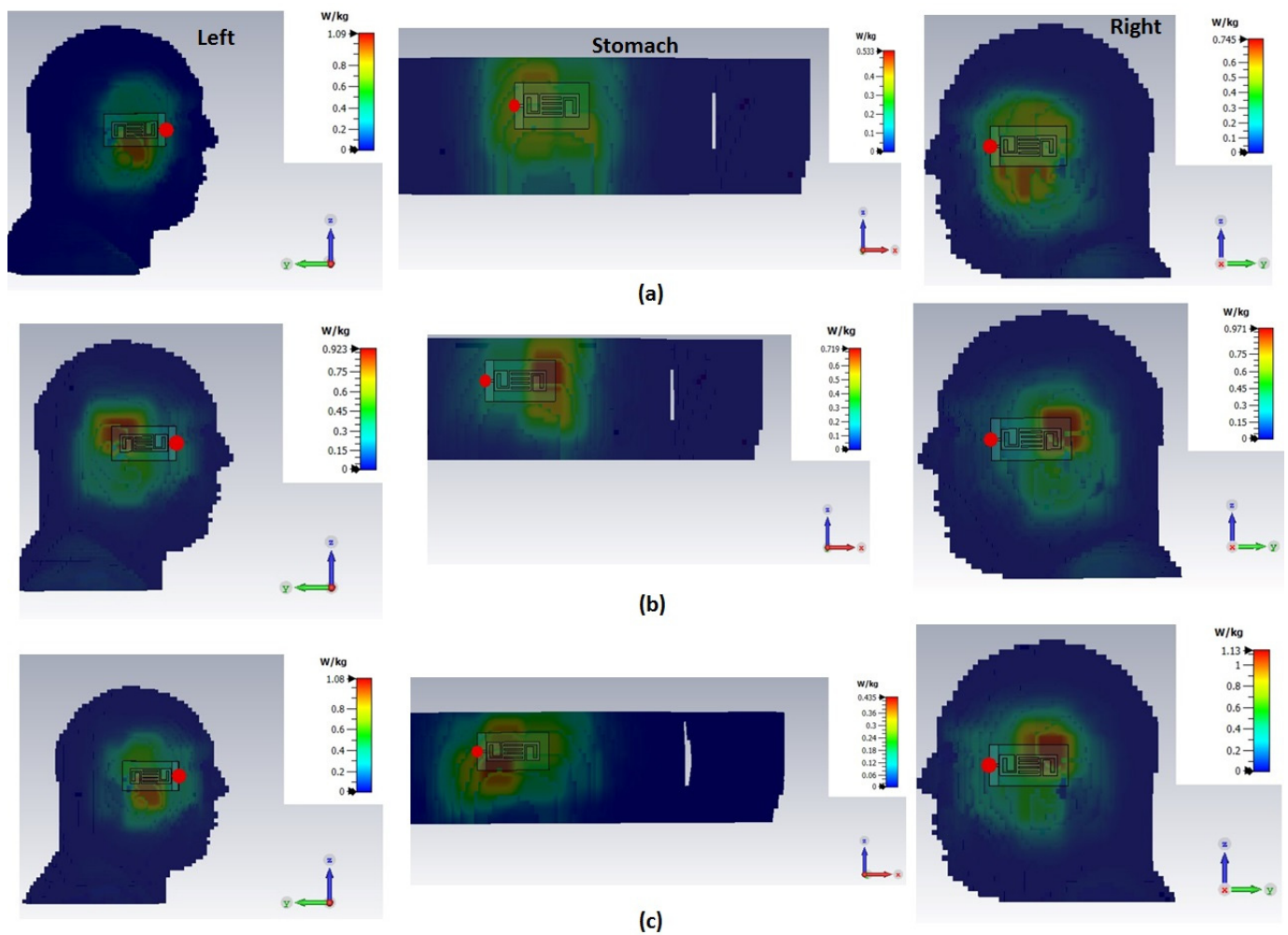

Figure 18. The simulated antenna efficiency. (**a**) Radiation. (**b**) Total.

Figure 19 demonstrates the SAR levels of the radiator at three different bands, considering various positions on the human body (stomach, left and right head). The antenna was subjected to a 100 mW input power. Simulated SAR levels over 10 g of the stomach, left and right head are presented in Figure 19a–c. Notably, the antenna exhibits SAR levels at the left head of 1.09, 0.92, and 1.08 W/kg at 2.45, 3.5, and 5.8 GHz, respectively. Similarly, at the stomach, SAR levels stand at 0.53, 0.73, and 0.44 W/kg for the same frequencies. Furthermore, at the right head, SAR levels are 0.74, 0.97, and 1.13 W/kg at respective bands—all of which fall below the accepted limits.
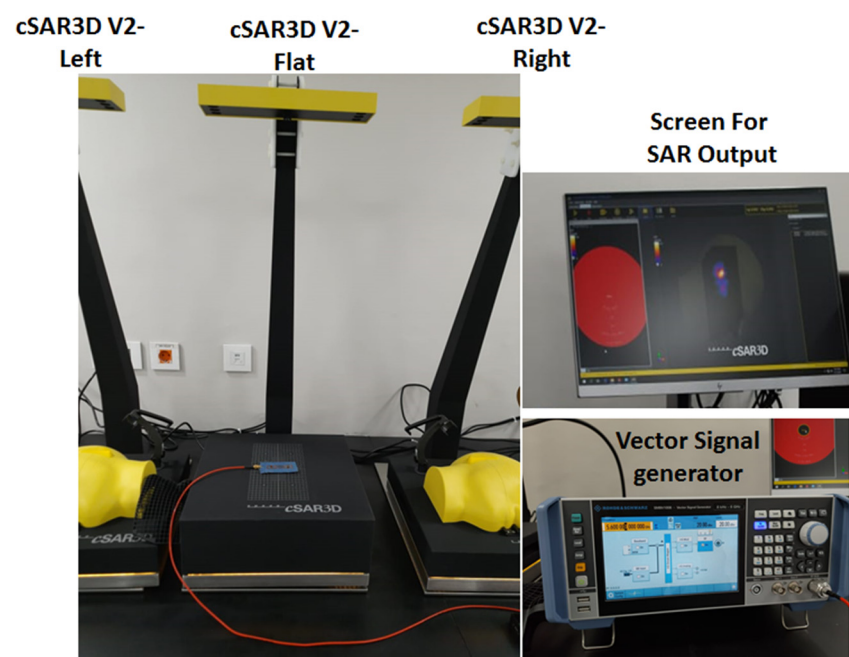
The cSAR3D system, depicted in Figure 20, was employed to assess antenna SAR levels at several positions, including the stomach, left, and right head. Renowned for its capability to swiftly measure both real-time full SAR distribution and its average, the cSAR3D system utilizes flat phantoms for the left and right heads.

The measurement process involved several steps: firstly, placing the system on a stable, non-metallic surface; secondly, connecting the power and establishing necessary connections with the measured equipment or software; thirdly, linking the power source with an appropriate level to the antenna or phantom; fourthly, monitoring the measurement progress to ensure successful completion; finally, once measurements were concluded, SAR data were extracted from the system, transferred to analysis software for additional processing, and displayed on the monitor. These procedural steps, as illustrated in Figure 21, were specifically tailored for the wearable antenna. Extracted SAR levels from the system, focusing on the stomach, and a human head, are presented in Figure 22.

The outcomes of the SAR levels are shown in Table 2. The tested SAR does not exceed the safety standard limits. Nevertheless, a minor variance exists between the measured outcomes and the simulation due to the direct integration of the antenna with the phantom model.

Figure 19. The SAR distribution of the human head (left and right) and stomach at (**a**) 2.45 GHz, (**b**) 3.5 GHz, and (**c**) 5.8 GHz.
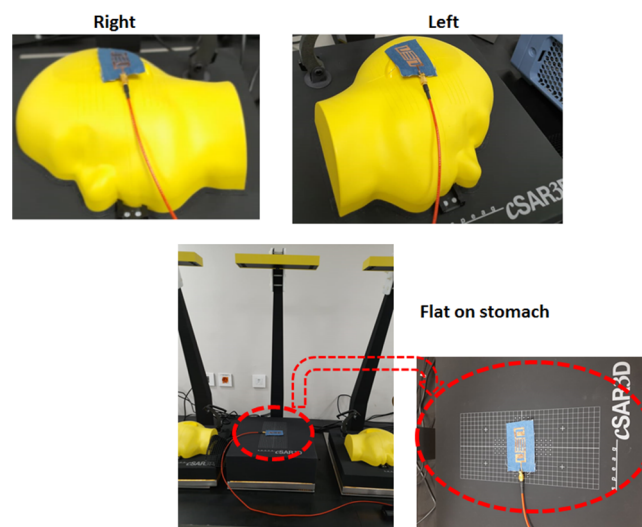

Figure 20. The SAR measuring cSAR3D system.

Figure 21. SAR testing setup of the wearable antenna.
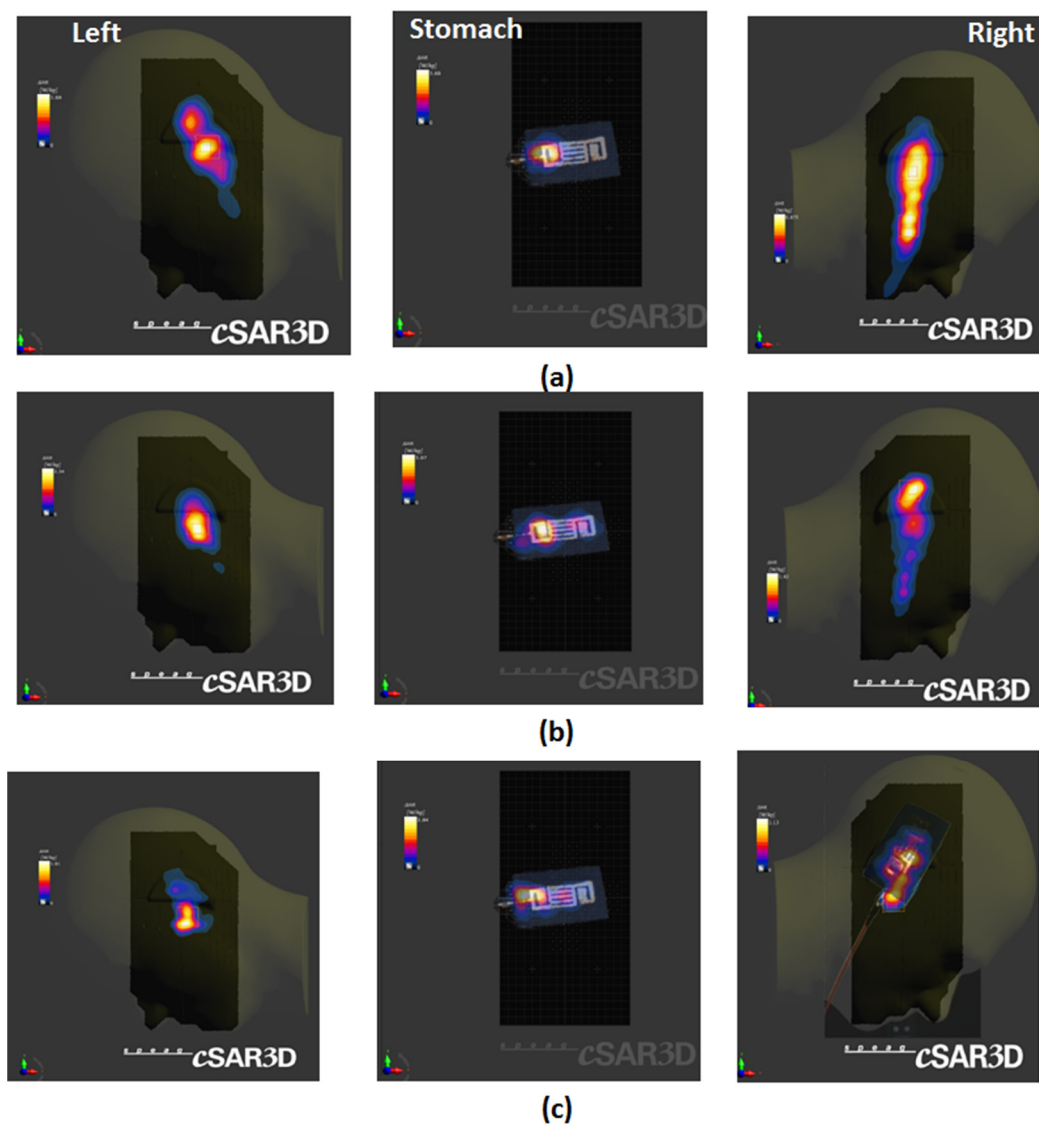

Figure 22. The measured SAR levels on the human head and stomach at (**a**) 2.45 GHz, (**b**) 3.5 GHz, and (**c**) 5.8 GHz.

Table 2. The SAR for the presented design by FCC (1 g) and ICNIPR (10 g) 3 mm from the model.

Freq.	SAR Value (w/kg)											
	Stomach				Left Head				Right Head			
	10 g		1 g		10 g		1 g		10 g		1 g	
	S *	M *	S	M	S	M	S	M	S	M	S	M
2.45	0.53	0.69	1.25	1.56	1.09	1.21	1.26	1.49	0.74	0.92	0.95	1.02
3.5	0.73	0.88	1.04	1.17	0.92	1.08	1.03	1.19	0.97	1.04	1.15	1.23
5.8	0.44	0.63	0.98	1.21	1.08	1.13	1.12	1.23	1.13	1.18	1.23	1.31

* S: Simulated; M: Measured.

Table 3 presents a comparison of the suggested dual-wideband wearable antenna with other antennas of similar design. The distinctive contribution is summarized as follows:

1. The SAR analysis involves both simulation and measurement on a human voxel, a distinction from the antennas discussed in references [16–22].
2. The antenna attained the broadest impedance bandwidth when compared to other dual-band wearable antennas.
3. Denim, chosen as the substrate, surpasses other materials like rubber, cellulose laurate, and polyimide in wearable applications due to its exceptional combination of lightweight construction, flexibility, and cost-effectiveness for printing.
4. Despite its flexible nature, the antenna achieved commendable gain and maintained a comparable size to other antennas.

Table 3. Comparison of proposed dual-wideband antenna and other analogous designs.

Ref	% Bandwidth	Substrate	Size (mm³)	Gain (dBi)	Bending Analysis	SAR Analysis	Application
[16]	20.40 (2.2–2.7 GHz), 21.15 (4.65–5.75 GHz)	nitrile butadiene rubber fabric (Multilayer Structure)	40 × 50 × 4.6	1.5, 1.7	No	Simulation study	Body-centric wireless communications
[17]	10.52 (2.25–2.5 GHz), 21.26 (5.21–6.45 GHz)	Felt	44.1 × 44.1 × 5	−0.67, 7.4	Yes	Simulation study	WBAN
[18]	3.7 (2.35–2.44 GHz), 5.15 (5.67–5.97 GHz)	Rogers Duroid RO3003 (Semi Flexible)	41 × 44 × 1.52	3.74, 5.13	Yes	Simulation study	WBAN
[19]	5.7% (2.4–2.54 GHz), 3.78% (5.72–5.94 GHz)	Rogers RT/Duroid 5880 (Semi Flexible)	19 × 12 × 0.508	2.1, 3.5	Yes	Simulation study	WBAN
[20]	7.56 (890–960 MHz), 9.73 (171–188 MHz)	Rubber	70 × 85 × 1.64	7.46, 8.13	No	Simulation study	Telemonitoring
[21]	2.86 (2.41–2.48 GHz), 3.10 (5.70–5.88 GHz)	cellulose laurate	58 × 54 × 0.4	3, 5.3	Yes	Simulation study	WBAN

Table 3. *Cont.*

Ref	% Bandwidth	Substrate	Size (mm³)	Gain (dBi)	Bending Analysis	SAR Analysis	Application
[22]	37.22 (2.23–3.25 GHz), 38.43 (4.54–6.70 GHz)	polyimide	17 × 29 × 0.15	1.7, 8.1	Yes	Simulation study	WBAN
Proposed	58.06 (2.2–4 GHz), 61.43 (5.3–10 GHz)	Denim	40 × 77 × 0.6	3, 4	Yes	Simulation and measured	WBAN

Furthermore, several applications for future work are discussed, encompassing both wearable electronic skins and optogenetic neural modulation [25,26]. These recent advances in wearable electronic skins offer promising integration into comfortable, lightweight devices, enhancing wearable sensors and optoelectronics. However, challenges like complex fabrication, high costs, and durability hinder their widespread use. A scalable electrospun patterned solution presents mechanically robust nano-microfibers, enabling durable health sensors, pressure sensors, electroluminescent displays, and flexible OLEDs [25]. In parallel, the optogenetic modulation of brain neural activity has surged, integrating optical and electrical modes. Key focuses include controlling illumination coverage, developing light-activated modulators, and enhancing wireless delivery and data transmission. Biocompatible electrodes with improved optoelectrical performance multiplexed addressing, and soft system integration enable spatiotemporal neural response imaging with minimal artifacts, paving the way for nonpharmacological neurological disease treatments [26].

5. Conclusions

This paper presents a dual-wideband monopole radiator ingeniously engineered on a flexible denim substrate, specifically tailored for wireless body area network (WBAN) applications in healthcare. It underscores denim's exceptional attributes, emphasizing its lightweight nature, remarkable flexibility, and cost-effectiveness compared to alternative substrates. The antenna's standout feature lies in its expansive bandwidth coverage, which not only ensures comprehensive monitoring capabilities but also maintains stability even under bending conditions. Moreover, the antenna successfully passes rigorous safety assessments, particularly in specific absorption rate (SAR) testing using the cSAR3D system, affirming its adherence to established safety standards. This innovative solution represents a significant stride in addressing critical deficiencies observed in current wearable antenna technologies. By bridging these gaps, it plays a pivotal role in propelling the frontiers of healthcare technology forward, particularly in the realm of remote patient monitoring. Ultimately, the introduction of this dual-wideband monopole radiator marks a notable advancement in the field, promising enhanced efficiency, reliability, and effectiveness in healthcare applications. It sets a new standard for wearable antennas, offering a compelling avenue for future research and development in the pursuit of improved healthcare outcomes and patient well-being.

Author Contributions: Conceptualization, M.A.A., A.D. and A.A.I.; methodology, M.F.A., A.A.I. and A.D.; software, M.F.A., A.A.I. and A.D.; validation, M.I.A., M.A.A. and A.A.I.; investigation, M.F.A., A.A.I. and A.D.; fabrication, and measurements, M.I.A.; writing original draft preparation, A.D., A.A.I. and M.A.A.; writing—review and editing, M.F.A., M.I.A. and M.A.A. All authors have read and agreed to the published version of the manuscript.

Data Availability Statement: All data generated or analyzed during this study are included in this article.

Conflicts of Interest: The authors declare no conflicts of interest.

References

1. Verena, M.; Radouchová, M.; Soukup, R.; Hipp, S.; Blecha, T. Wearable textile antennas: Investigation on material variants, fabrication methods, design and application. *Fash. Text.* **2024**, *11*, 9.
2. Ahmed, M.I.; Ahmed, M.F. Study of Bending, Crumpling, and SAR for a Multi-band Wearable Fractal Antenna for Telemedicine Applications. *Int. J. Microw. Opt. Technol.* **2019**, *14*, 240–246.
3. Ayd RSaad, A.; Hassan, W.M.; Ibrahim, A.A. A monopole antenna with cotton fabric material for wearable applications. *Sci. Rep.* **2023**, *3*, 7315. [CrossRef]
4. Pendli, P.; Basha, M.M.; Gundala, S.; Syed, J. Development of Wearable Textile MIMO Antenna for Sub-6 GHz Band New Radio 5G Applications. *Micromachines* **2024**, *15*, 651.
5. Ibrahim, A.A.; Ahmed, M.I.; Ahmed, M.F. A systematic investigation of four ports MIMO antenna depending on flexible material for UWB networks. *Sci. Rep.* **2022**, *12*, 14351. [CrossRef] [PubMed]
6. Arpan, D.; Hsu, H.-T.; Yousef, B.M.; Ameen, A.M.; Tsao, Y.-F.; Ibrahim, A.A. UWB Connected Ground Transparent 4-Port Flexible MIMO Antenna for IoT Applications. *IEEE Internet Things J.* **2023**, *11*, 12475–12484.
7. Arpan, D.; Palandoken, M.; Kulkarni, J.; Byun, G.; Nguyen, T.K. Wideband flexible/transparent connected-ground MIMO antennas for sub-6 GHz 5G and WLAN applications. *IEEE Access* **2021**, *9*, 147003–147015.
8. Gohar, V.; Keshtkar, A.; Daryasafar, N.; Naser-Moghadasi, M. Microstrip Sierpinski fractal carpet for slot antenna with metamaterial loads for dual-band wireless application. *AEU Int. J. Electron. Commun.* **2018**, *84*, 93–99.
9. Walaa, M.H.; Saad, A.A.R.; Ibrahim, A.A. Ultra-wideband flexible antenna applicable for dual-band on-body communications. *Int. J. Microw. Wirel. Technol.* **2023**, *15*, 609–622.
10. Shailesh, J.; Srivastava, G.; Purwar, R. Bending and SAR analysis on UWB wearable MIMO antenna for on-arm WBAN applications. *Frequenz* **2021**, *75*, 177–189.
11. Gao, G.-P.; Yang, C.; Hu, B.; Zhang, R.-F.; Wang, S.-F. A Wearable PIFA With an All-Textile Metasurface for 5 GHz WBAN Applications. *IEEE Antennas Wirel. Propag. Lett.* **2018**, *18*, 288–292. [CrossRef]
12. Zheng, Y.; Zhang, K.; Chen, J.; Yan, S. Compact monopole antenna for wireless body area network, wireless local area network, and ultrawideband applications. *Int. J. RF Microw. Comput. Aided Eng.* **2021**, *31*, e22546. [CrossRef]
13. Kanagasabai, M.; Sambandam, P.; Alsath, M.G.N.; Palaniswamy, S.; Ravichandran, A.; Girinathan, C. Miniaturized Circularly Polarized UWB Antenna for Body Centric Communication. *IEEE Trans. Antennas Propag.* **2021**, *70*, 189–196. [CrossRef]
14. Chen, P.; Wang, D.; Liu, L.; Wang, L.; Lin, Y. Design of UWB Wearable Conformal Antenna Based on Jean Material. *Int. J. Antennas Propag.* **2022**, *2022*, 4886844. [CrossRef]
15. Simorangkir, R.B.; Kiourti, A.; Esselle, K.P. UWB Wearable Antenna With a Full Ground Plane Based on PDMS-Embedded Conductive Fabric. *IEEE Antennas Wirel. Propag. Lett.* **2018**, *17*, 493–496. [CrossRef]
16. Abdullah, A.-S.; Al-Ghamdi, A.; Dishovsky, N.; Atanasov, N.; Atanasova, G. Design and performance analysis of dual-band wearable compact low-profile antenna for body-centric wireless communications. *Int. J. Microw. Wirel. Technol.* **2018**, *10*, 1175–1185.
17. Zhang, K.; Soh, P.J.; Yan, S. Design of a compact dual-band textile antenna based on metasurface. *IEEE Trans. Biomed. Circuits Syst.* **2022**, *16*, 211–221. [CrossRef] [PubMed]
18. Umar, M.; Shah, S.M.; Majid, H.A.; Mahadi, I.A.; Rahim, M.K.A.; Yahya, M.S.; Abidin, Z.Z. Design and Analysis of a Compact Dual-Band Wearable Antenna for WBAN Applications. *IEEE Access* **2023**, *11*, 30996–31009.
19. Le, T.T.; Yun, T.-Y. Miniaturization of a dual-band wearable antenna for WBAN applications. *IEEE Antennas Wirel. Propag. Lett.* **2023**, *19*, 1452–1456. [CrossRef]
20. Shirvani, P.; Khajeh-Khalili, F.; Neshati, M.H. Design investigation of a dual-band wearable antenna for tele-monitoring applications. *AEU Int. J. Electron. Commun.* **2021**, *138*, 153840. [CrossRef]
21. Sid, A.; Cresson, P.-Y.; Joly, N.; Braud, F.; Lasri, T. A flexible and wearable dual band bio-based antenna for WBAN applications. *AEU Int. J. Electron. Commun.* **2022**, *157*, 154412. [CrossRef]
22. Zheng, H.; Cui, W.; Liu, R.; Li, Z.; Fan, C.; Wang, M.; Li, E. Design of flexible dual-band antenna and metamaterial structure for wearable body area network. *Int. J. RF Microw. Comput. Eng.* **2022**, *32*, e23083. [CrossRef]
23. Ismail, A.M.; Ahmed, M.F. A Dual-Band Flexible Wearable Antenna Integrated on a Smart Watch for 5G Applications. In *Fundamental and Supportive Technologies for 5G Mobile Networks*; IGI Global: Hershey, PA, USA, 2020; pp. 77–101.
24. Ahmed, M.I.; Ahmed, M.F.; Shaalan, A.-E.A. Novel electro-textile patch antenna on jeans substrate for wearable applications. *Prog. Electromagn. Res. C* **2018**, *83*, 255–265. [CrossRef]

25. Veeramuthu, L.; Cho, C.-J.; Liang, F.-C.; Venkatesan, M.; Kumar G, R.; Hsu, H.-Y.; Chung, R.-J.; Lee, C.-H.; Lee, W.-Y.; Kuo, C.-C. Human skin-inspired electrospun patterned robust strain-insensitive pressure sensors and wearable flexible light-emitting diodes. *ACS Appl. Mater. Interfaces* **2022**, *14*, 30160–30173. [CrossRef]
26. Xu, S.; Momin, M.; Ahmed, S.; Hossain, A.; Veeramuthu, L.; Pandiyan, A.; Kuo, C.; Zhou, T. Illuminating the Brain: Advances and Perspectives in Optoelectronics for Neural Activity Monitoring and Modulation. *Adv. Mater.* **2023**, *35*, 2303267. [CrossRef]